18

MECHANICS OF A RIVER MEANDER

William E. Dietrich

Introduction

Since 1976, Thomas Dunne, J. Dungan Smith and I have been studying flow and sediment transport in meanders of Muddy Creek. Our principal goal has been to discover what processes control the equilibrium bed morphology in a river bend during a period of constant discharge. Nine models have been proposed to predict the bed morphology of a channel of a given curvature, width, discharge and sediment size (Yen, 1970; El-Khudairy, 1970; Allen, 1970a; Engelund, 1974; Gottlieb, 1976; Kikkawa et al., 1976; Bridge, 1977; Zimmerman and Kennedy, 1978; Odgaard, 1981). The assumptions in all these models are similar, and can be illustrated in the diagram from Allen (1970,b) reproduced in Figure 1.

Flow through a bend experiences a centrifugal force that accelerates the faster moving fluid near the water surface toward the outer bank, causing the water surface to rise toward the outer bank and lower toward the inner bank. This generates a cross-stream pressure gradient that forces the slower fluid near the channel bed inward relative to the surface flow. In this manner, a secondary circulation is established (Fig. 1). Inward component of velocity adds to the downstream component and a resultant, diagonally inward velocity is produced. A boundary shear stress vector is formed similarly. Particles travelling on the bed are forced toward the outer bank by the cross-stream component of gravity and are forced inward by the cross-stream boundary shear stress. In most models it has been assumed that the equilibrium bed morphology is established when these opposing forces balance, so that the net cross-stream force is equal to zero, and the particles follow a path parallel to the banks. This assumption has gained wide acceptance amongst geomorphologists and sedimentologists and is now being presented in textbooks as a fundamental balance of forces controlling bed morphology in river meanders (i.e., Embleton and Thornes, 1979).

During the field trip I will explain in greater detail processes of flow and sediment transport through a meander. Data on these processes demonstrate that the assumptions of the above models are incorrect. I will conclude by presenting an alternative model for equilibrium bed morphology.

Study Reach

We have attempted to use laboratory techniques and procedures when possible to obtain a complete set of field data on the flow, boundary shear stress and sediment transport fields during a period of constant discharge through the meander. Muddy Creek is well suited for such work. During the late spring and early summer the channel receives irrigation return flow and experiences long periods of relatively constant high discharge, permitting detailed measurement of flow and sediment transport fields at constant stage. During the period 1976-1980, three of the years had the same constant stage, allowing combination of data. The discharge for this stage was 1.1 m^3/sec, 70% of bankfull discharge. During this discharge the flow carried very little suspended load and because of the relatively shallow depth of the stream, the bed could easily be seen. At this stage the stream transports a coarse sand bedload in the form of well developed quasi-two-dimensional

sand waves in the curved reaches and complex three-dimensional dune fields in the crossings (Fig. 2). A large portion of the sediment in the channel originates from bank erosion in outwash terraces (Andrews, 1977), so the supply of sediment is not exhausted early in the high flow season. This constant supply of water and sediment permits the development and maintenance of an equilibrium morphology during a period of constant discharge.

At the measurement site the stream has a drainage area of about 235 km^2 and a gradient of 0.0014. Bankfull discharge, mean width and mean depth are respectively 1.6 m^3/sec, 5.5 m and 0.5 m, and the maximum pool depth at this stage is 1.1 m. Figure 3 shows the study reach as it appeared in 1976, and Figure 4 shows that significant bank migration (1.7 m in 4 years) has occurred in the center of the bend. The first three years of channel migration appear to have caused relatively small changes in the flow and sediment transport fields. Nearly all of the data used in this analysis were collected simultaneously in 1978.

The small size of the stream permitted construction of a continuous railing along both banks upon which wooden bridges could be placed and freely moved to any position in the channel. This allowed the precise placement of laboratory scale instruments in the flow and on the bed.

Flow and Boundary Shear Stress

1. Theoretical framework

To model the development and maintenance of the point bar, we need to understand how flow is influenced by both channel curvature and downstream changes in channel topography. In particular, we need to predict the magnitude and direction of boundary shear stress through the meander. The boundary shear stress transports the bed material and, thus, ultimately controls the shape of stream beds. As part of their examination of the effects of channel geometry on flow processes in rivers, Smith and McLean (in prep.) wrote the equation of motion for fluid flow in a right handed, orthogonal, curvilinear coordinate system that follows the channel centerline. They vertically averaged the resulting equations and arrived at the following downstream and cross-stream force balance equations.

$$(\tau_{zs})_b = \frac{-\rho\, g\, h}{1-N}\frac{\partial E}{\partial s} - \frac{1}{1-N}\,\rho\,\frac{\partial \langle u_s^2\rangle h}{\partial s} - \rho\,\frac{\partial \langle u_s u_n\rangle h}{\partial n} + 2\rho\,\frac{\langle u_s u_n\rangle h}{(1-N)\,R} \qquad (1)$$

$$(\tau_{zn})_b = -\rho\, g\, h\,\frac{\partial E}{\partial n} - \rho\,\frac{\langle u_s^2\rangle h}{(1-N)R} - \frac{1}{1-N}\,\frac{\rho\,\partial \langle u_s u_n\rangle h}{\partial s} - \rho\,\frac{\partial \langle u_n^2\rangle h}{\partial n} + \frac{\rho \langle u_n^2\rangle h}{(1-N)R} \qquad (2)$$

Here the s-axis points downstream along the centerline, z is a nearly vertical axis, and n is the cross-stream axis, positive toward the left bank. The scale factors for derivatives with respect to the cross-stream and vertical curvilinear coordinates are unity, but that associated with the downstream coordinate is $1 - n/R = 1 - N$. This scale factor compares an arc length with a radius of curvature R measured along the channel centerline to an arc length measured along any other line of constant n.

$(\tau_{zs})_b$ and $(\tau_{zn})_b$ are the downstream and cross-stream components of boundary shear stress, h and E are the depth of flow and elevation of the water surface with respect to an arbitrary datum, and u_s and u_n are the downstream and cross-stream components of the velocity. The bracket indicates that the enclosed quantity has been vertically averaged. The downstream force balance equation (1) states that the boundary shear stress is equal to the sum of forces caused by the downstream pressure gradient force (the first term on the right-hand side of the equation), by the change in momentum of the downstream flow in the downstream and cross-stream directions (next two terms in the equation) and by a force associated with channel curvature and secondary circulation (fourth term on the right-hand side). The cross-stream force balance (2) states that the cross-stream boundary shear stress is equal to the sum of forces caused by the cross-stream pressure gradient, by the centrifugal acceleration of the flow (second and fifth terms on the right-hand side) and by the change in momentum of the cross-stream flow (third and fourth terms). To arrive at the force balance in equation (1), Smith and McLean used the vertically averaged continuity equation for steady flow, which can be written as

$$\langle u_n \rangle h = - \frac{1}{1-N} \int_{-w/2}^{n} \frac{\partial \langle u_s \rangle h}{\partial s} \, dn \qquad (3)$$

Equation (1) and (2) indicate that to study this problem experimentally, careful measurements of the flow field and water surface topography must be made throughout the study reach so that individual terms can be computed accurately. Further, independent measurements of the boundary shear stress pattern must be obtained to serve as a test of the predicted values.

2. Field techniques

The magnitude and direction of velocity were obtained at nine sections through the meander by means of 12 pairs of 4 cm diameter rotor-type current meters positioned at regular intervals through the water column and across the channel. These current meters were suspended from wooden bridges across the channel and the output from all 24 current meters was stored simultaneously by multichannel digital counters. Velocity was monitored for 10 minute intervals over two-hour periods at about 60 locations in each of nine sections. Water surface topography was surveyed by wading and using a survey rod with a sharply pointed base.

The pattern of boundary shear stress through the meander was computed from 110 velocity profiles made with a 6 by 4 cm electromagnetic current meter and fitted to the standard logarithmic equation: $u = (u_*/k) \ln z/z_0$. u is the velocity at an elevation z above the bed, u_* is the shear velocity, equal to square root of the boundary shear stress divided by the water density, k is von Karman's constant, (0.43), and z_0 is a roughness parameter. Because of the mobility and complexity of the bed this technique has large errors associated with it. In addition it is very difficult to eliminate form drag effects caused by the bedforms. As an alternative we developed a model to predict the boundary shear stress from a single velocity measurement near the bed. The model is based on predictions of the hopping height of bedload particles and correlation of this hopping height with the roughness parameter (z_0). This relation exists because the hopping of particles off the bed extracts momentum from the near boundary fluid, increasing the resistance to motion.

3. Summary of results

As flow enters the bend it experiences a progressively increasing centrifugal force as the radius of curvature decreases. This causes the water surface to rise near the outer bank, lower near the inner bank and generates a steep cross-stream pressure gradient. Between sections 12 and 18 the cross-stream slope was 2.7 times greater than the downstream slope. The cross-stream pressure gradient does not, however, force an inward velocity near the bed across the entire channel width, as is traditionally assumed to occur. Instead the rapid shoaling of the flow over the upstream end of the point bar causes a large net outward discharge and an outward velocity near the bed in the upstream part of the bend (Figs. 5-7). Downstream of the minimum point bar depth, the inward velocity near the bed spreads across the entire channel width. The classic secondary circulation pattern of outward velocity at the surface and inward near the bed was confined to about 20 to 30% of the channel width through the center and downstream end of the bend. Previous field studies, including those by Rozovskii (1961) and Bridge and Jarvis (1976), have failed to recognize this pattern because of incorrect use of the continuity equation.

The downstream velocity field consists of a high velocity core that shifts from the inside bank to the outside bank through the bend (Fig. 5). This core tends to follow the zone of the greatest downstream pressure-gradient force, the position of which in turn is largely controlled by the curvature of the channel. The outward transfer of momentum over the point bar, caused by the shoaling of the flow, contributes to the rapid crossing of the high velocity core.

The boundary shear stress fields computed from the velocity profiles and from the single-velocity model were similar and consisted of a zone of high boundary shear stress that shifted from the inside bank, across the top of the point bar, and toward the outside bank through the bend (Figs. 8 and 9). The average boundary shear stress causing sediment transport was 16 dynes/cm^2. The form-drag resistance from dunes increased the boundary shear stress to 30 dynes/cm^2 and the additional resistance to flow caused by channel curvature and bar and pool topography caused the total boundary shear stress to be 55 dynes/cm^2.

Analysis of the flow data indicate that, as Yen and Yen (1971) had found in a laboratory study, the momentum change terms in equation (1) are generally much larger than the downstream pressure-gradient force. In the upstream part of the bend, however, the two terms are of opposite sign and tend to cancel. In the downstream end of the bend, where the momentum change terms may be of the same sign, they are probably smaller in magnitude. Because of this there tends to be a positive correlation between the downstream pressure-gradient force and downstream boundary shear stress. As a result, the general pattern of downstream boundary shear stress in a river meander can be roughly estimated from measurement of the water surface topography and from calculation of the downstream pressure gradient. These measurements alone, however, cannot be sufficiently accurate to be used in quantitative modelling of sediment transport processes.

Sediment Transport Through the Study Reach

1. Field techniques

During periods of constant high discharge bedforms develop a well-defined pattern through the study reach (Figs. 10 and 11). Obliquity of bedform to the flow direction causes a current along the trough toward the downstream end of

the bedform (Fig. 12) that in many cases is capable of transporting sediment (see discussion in paper by Fredsøe, 1974, or by Dietrich et al., 1979 for explanation of this effect). Bedforms exert a strong influence on the direction and magnitude of bedload transport through the bend. To define this influence quantitatively, we measured, simultaneously, bedform migration and the magnitude and direction of bedload transport at nine sections through the reach. We used a 2 cm orifice Helley-Smith type bedload sampler and noted its orientation on the bed with a compass. At a point on the bed, sediment transport ranged over several orders of magnitude as bedforms travelled downstream. This variation required sampling repeatedly from dune crest to trough over at least one and up to four dunes. On average we collected 18 samples at a position on the stream bed and 740 samples were used to define the structure of the bedload tranpsort field at nine sections through the reach. Bedform and bedload transport fields compared well, and, for the nine sections, the average transport (mean ± standard deviation) was 128.5 gm/sec ± 32.7 gm/sec for bedload versus 131.6 gm/sec ± 21.1 gm/sec for bedform transport. We also computed the bedload transport from our observed boundary shear stress and the Yalin bedload expression (Yalin, 1963). For eight sections the predicted bedload transport averaged 123 gm/sec. Suspended load transport determined with a USDH-48 sampler was only on average 14 gm/sec ± 6.8 gm/sec.

The settling velocity distribution of each bedload sample was determined so that the transport vector of seven settling velocity classes through the bend could be computed. We also painted sediment and mapped particle paths throughout the bend. Figures 13 through 17 show some of the results of our measurements and will be used in the following summary of transport processes through the bend.

2. Summary of results

The pattern of dune migration and sediment transport through the bend can be divided into three successive reaches, reflecting the changing pattern of boundary shear stress. In the upstream part of the bend (sections 12-18, Figs. 8 and 9), a zone of maximum boundary shear stress lies near the inside (right) bank. The major bedforms entering the bend at section 12 travel most rapidly in this zone, and their crests slowly rotate and become oblique to the mean flow direction with their downstream ends near the right bank. These dunes generate an inward, troughwise transport of sediment that counteracts the weak outward transport on the stoss side of dunes caused by the shoaling of the flow over the point bar. The bedload follows a zig-zag path, but a net inward transport of sediment occurs. In this upstream reach, the coarsest sediment in transport and the zone of maximum sediment transport lie close to the inside bank in the zone of maximum boundary shear stress.

In the center of the bend (section 19 to 20), the zone of maximum boundary shear stress shifts across the channel into the deep water near the center line of the channel. The major bedforms near the inside bank on the shallow part of the point bar thin downstream and, although strongly oblique to the mean flow direction, generate a weak inward current capable of transporting only fine sediment. Large bedforms in the deep water grow and rotate downstream such that their crests are nearly perpendicular to the flow direction (Figs. 10 and 11). The fine sediment in the deep water is carried inward up the point bar surface by the inward secondary circulation caused by channel curvature, and by bedform orientation. Over the shallow part of the point bar, outward transport caused by shoaling of the flow over the point bar occurs. This carries coarse sediment in the zone

of maximum sediment transport outward to the abruptly steepening point bar slope (Figs. 11 and 17). Here sediment rolls and saltates down the troughs of those dunes with inside ends that curve back upstream (Fig. 17). Due to the steep slope across the channel, the coarse particles also will roll outward against the weak inward secondary circulation in the troughs of those dunes with crests almost perpendicular to the flow direction. The outward sediment transport shifts the zone of maximum downstream sediment transport toward the center of the channel. The position of maximum transport of fine sediment moves toward the inside bank, while the position of maximum transport of the coarsest sediment moves toward the outer bank (Fig. 13).

In the downstream end of the bend the maximum boundary shear stress shifts to the outer bank. The crests of the major bedforms travel most quickly in the zone of maximum boundary shear stress, and thus rotate with their downstream ends toward the outer (left) bank. The inward secondary circulation spreads across the entire channel width. The strong obliquity of the bedforms added to the steep cross-stream slope of the point bar causes significant transport by rolling and by troughwise currents toward the outside (left) bank. By the downstream end of the bend the boundary shear stress, bedload transport and median particle size are highest near the outer bank (Figs. 8, 14, and 15).

The sorting of sediment in a river meander results from the crossing of the bedload against an inward secondary circulation. Three processes contribute to the net transport of sediment across the channel. The outward secondary circulation caused by shoaling of flow over the point bar carries the sediment outward across the top of the point bar. Dune obliquity and the inward secondary circulation force flow inward from the pool and carry fine sediment to the top of the point bar. Rolling, avalanching and trough-wise currents along dunes sloping from the top of the point bar into the pool cause net outward transport against the inward secondary circulation throughout the downstream end of the bend.

Conclusion

Equilibrium bed morphology in a river channel develops when downstream increases or decreases in boundary shear stress are balanced with downstream convergences or divergences of sediment transport. The curvature and bed topography of a river meander cause the maximum boundary shear stress to be near the inside bank in the upstream part of the bend and to shift to the outside bank in the downstream end of the bend. Shoaling over the point bar, rolling, avalanching, and trough-wise transport along bedforms cause net outward transport that conveys sediment into the outward shifting zone of high boundary shear stress. The outward transport of the bed material against an inward secondary circulation sorts the sediment and establishes an equilibrium bed morphology.

Acknowledgements

Many have helped T. Dunne, J.D. Smith and me with field work and data analysis. We especially thank S. McLean, L. Reid, R. Spicer, P. Irle, L. Wilson, A. Nowell, M.A. Madej, M. Power, W. Smith, and F. Bardsley. This research was supported in part by NSF Grant ENG 78-16977, the Geological Society of America, the University of Washington Graduate School Research Fund, Corporation Fund of the Department of Geological Sciences, and Achievement Rewards for College Scientists.

References Cited

Allen, J.R. L., 1970a, Studies in fluviatile sedimentation: a comparison of fining-upwards cyclothems, with special reference to coarse member composition and interpretation: Jour. Sediment. Petrol., v. 40, 298-323.

Allen, J.R.L., 1970b, Physical processes in sedimentation, George Allen and Unwin Ltd., London, 248 pp.

Andrews, E.D., 1977, Hydraulic adjustment of an alluvial stream channel to the supply of sediment: Ph.D. dissertation, University of California, Berkeley, 152 pp.

Bridge, J.S., 1977, Flow, bed topography, grain size and sedimentary structure in bends: a three dimensional model: Earth Surface Processes, v. 2, p. 401-416.

Bridge, J.S. and Jarvis, J., 1976, Flow and sedimentary processes in meandering river South Esk, Glen Clova, Scotland: Earth Surface Processes, v. 1, p. 303-336.

Dietrich, W.E., Smith, J.D., Dunne, T., 1979, Flow and sediment transport in a sand bedded meander: Jour. Geol., v. 87, p. 305-315.

Dietrich, W.E., 1982, Flow, boundary shear stress and sediment transport in a river meander: Ph.D. dissertation, University of Washington, Seattle, 261 pp.

El-Khudairy, M., 1970, Stable bed profiles in continuous bends: Ph.D. dissertation, University of California, Berkeley.

Fredsøe, J., 1974, Rotational channel flow over small three-dimensional bottom irregularities: Jour. Fluid Mechanics, v. 66, p. 49-66.

Gottlieb, L., 1976, Three-dimensional flow pattern and bed topography in meandering channels: Institute of Hydrodynamics and Hydraulic Engineering, Technical University of Denmark, Series Paper 11, 79 pp.

Kikkawa, H., Ikeda, S., Kitagawa, A., 1976, Flow and bed topography in curved open channels, Jour. Hydraulics Div., Amer. Soc. Civil Engineers, v. 102, no. HY9, p. 1327-1342.

Odgaard, A.J., 1981, Transverse bedslope in alluvial bends: Jour. Hydr. Div. Amer. Soc. Civil Eng., v. 107, HY12, p. 1677-1694.

Rozovskii, I.L., 1961, Flow of water in bends of open channels: Israil Program for Scientific Translation; originally published by Academy of Sciences of the Ukranian SSR., 233 pp.

Valin, M.S., 1963, An expression for bed load transportation: Jour. Hydraulics Div., Am. Soc. Civ. Engineers, v. 89, no. HY3, p. 221-250.

Yen, C., 1970, Bed topography effect on flow in a meander: Jour. Hydraulics Div., Amer. Soc. Civ. Engineers, v. 96, no. HY1, p. 57-73.

Yen, C., and Yen, B., 1971, Water surface configuration in channel bends: Jour. Hydraulics Div., Amer. Soc. Civ. Engineers, v. 97, no. HY2, p. 303-321.

Zimmerman, C., and Kennedy, J.F., 1978, Transverse bed slopes in curved alluvial streams: Jour. Hydraulics Div., Amer. Soc. Civ. Engineers, v. 104, p. 33-48.

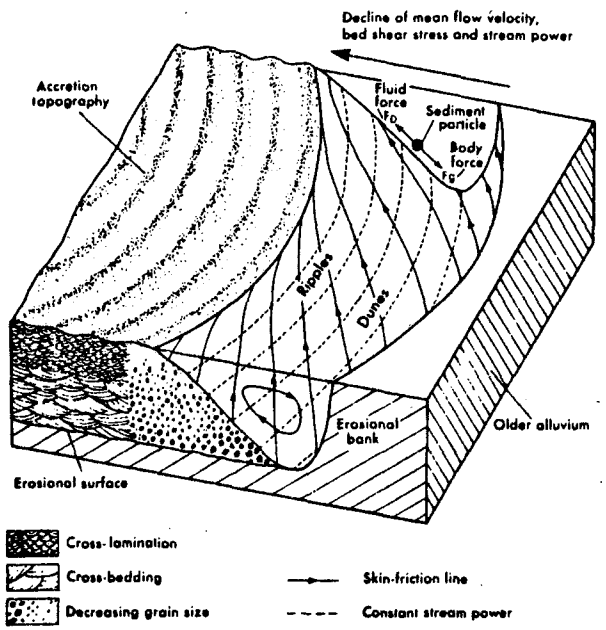

Figure 1. Processes controlling bed topography in a meandering river (Allen, 1970).

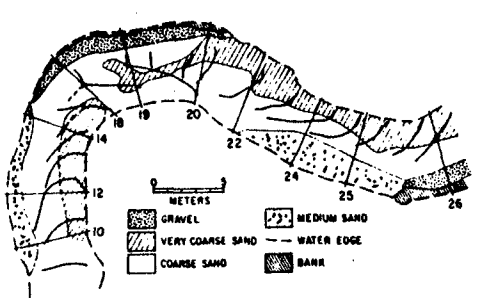

Figure 2. Texture of bed material at a range of discharge from 0.8–1.2 of bankfull and sketch of crest orientations of major bedforms at 0.7 of bankfull. The coarsest particles in the pool did not move at discharges of up to 1.3 times bankfull. In the zone between stations 14 and 19 the dashed lines indicate locations at which the slow moving outer extremities of crests merge as the high velocity of the inner crests increases the obliquity of the waves.

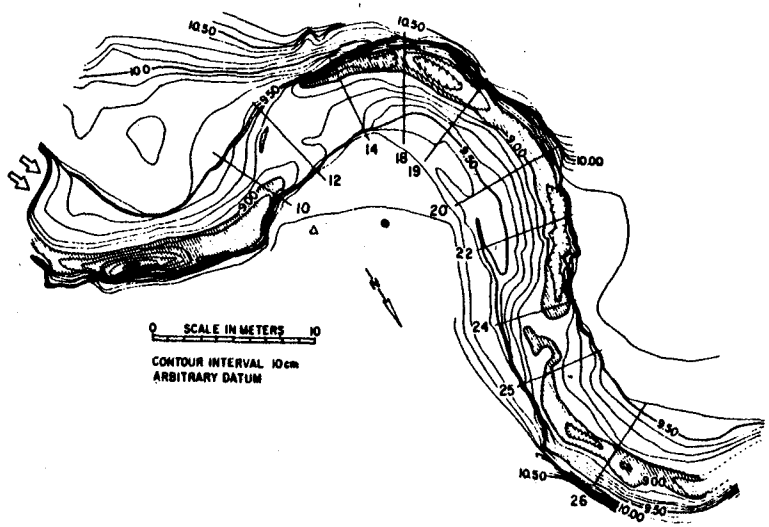

Figure 3. Topography of the study site. The pools have been shaded for emphasis.

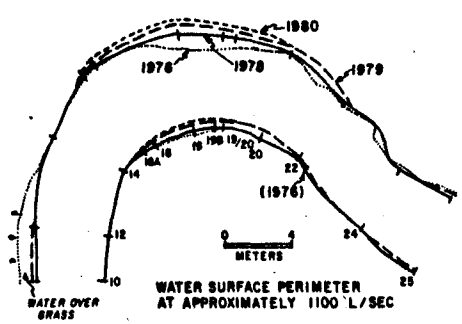

Figure 4. Water surface perimeter at approximately 1.1 m^3/sec for four years. Where line symbolizing the position of a bank in one year is absent, bank position was same as previous year. Very gentle topography partially invaded by grass made definition of the left edge of the water between sections 10 and 12 somewhat arbitrary.

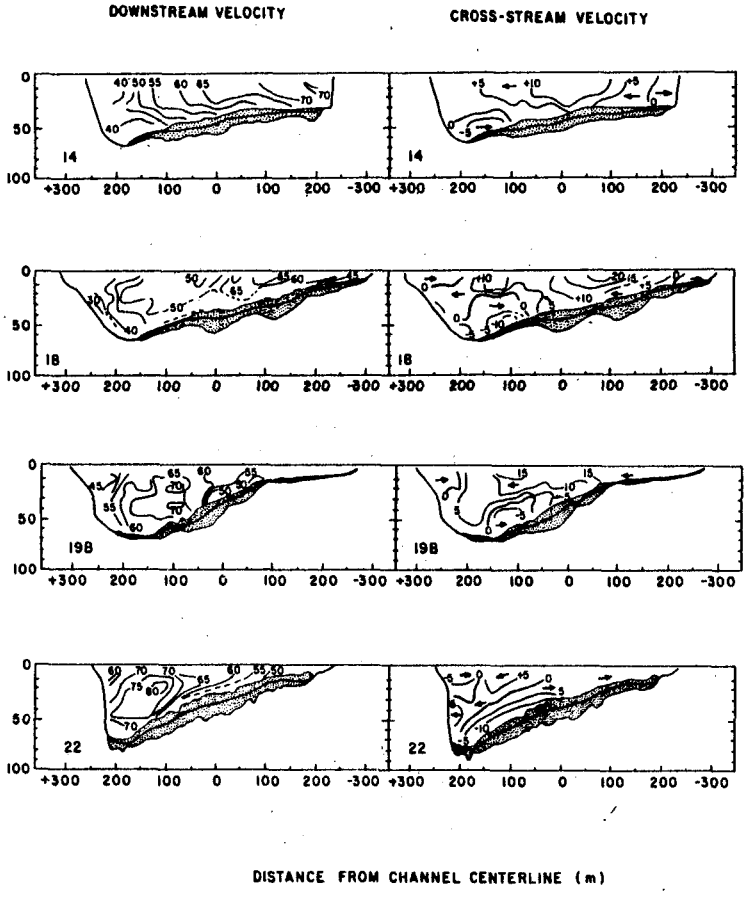

Figure 5. Downstream view of cross-sections of isovel surfaces, downstream and cross-stream components of flow. Contour interval is 5 cm/sec. Three lines at channel bed are the mean and range of depth determined from repeated measurement during a three-hour period. Arrows indicate direction across the channel. Large numbers in the lower corner are the section numbers. Vertical axis is depth in centimeters and horizontal axis is the distance from the channel centerline.

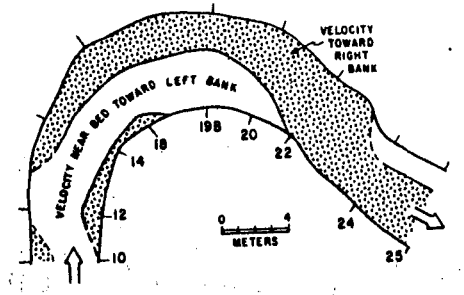

Figure 6. Direction of flow near the bed, as determined with current meter data. Left bank is the outside bank in the bend between sections 12 and 22 and the inside bank between sections 24 and 25.

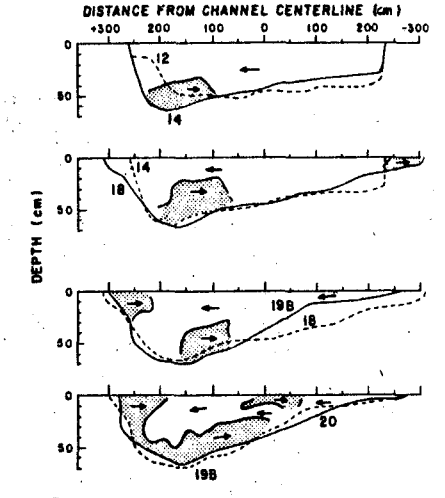

Figure 7. Distribution of inward and outward secondary circulation at successive cross-sections through the bend. Arrow indicates direction of motion in this downstream view of the sections. The channel outline represented by the solid line is the more downtream of the two sections portrayed and the pattern of secondary circulation applies to that section.

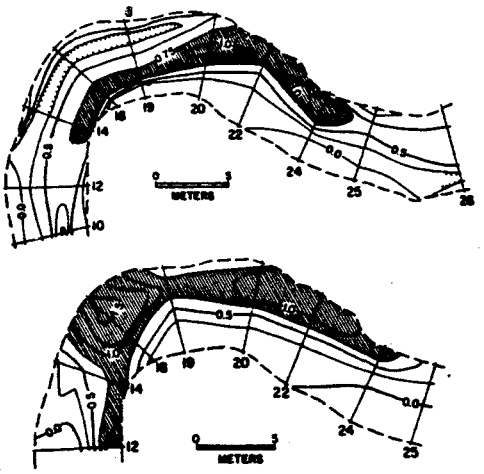

Figure 8. Boundary shear stress distribution. A: Measured distribution computed from velocity profiles. Discharge varied between 0.7 and 0.8 times bankfull during the measurements, and each computed stress is normalized by the mean total boundary shear stress in the downstream direction (calculated from equation (2)) between sections 12 and 24. The boundary shear stress is 50 dynes/cm^2 between stations 10 and 19 and 65 dynes/cm^2 between stations 20 and 26. B: Theoretical boundary shear stress distribution computed from equations (2) and (3). Magnitudes corrected to local boundary shear stress values by dividing by 2.11, and normalized by same values as in A.

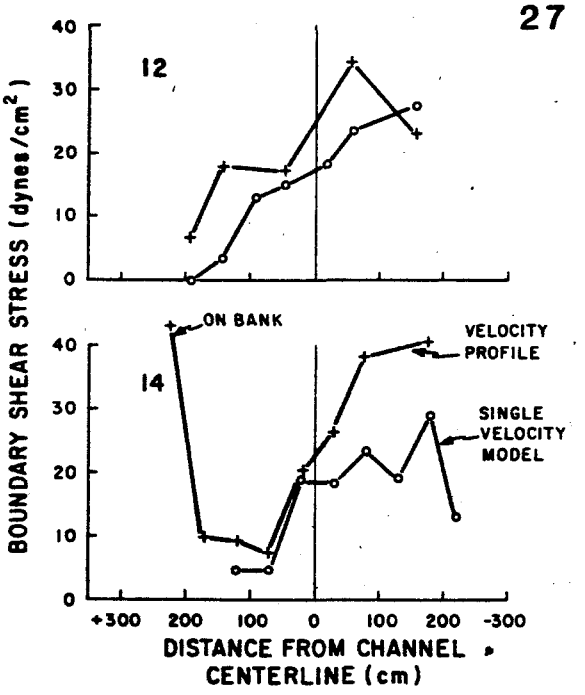

Figure 9. Comparison of boundary shear stress fields predicted by using a least squares fit of the logarithmic equation to velocity profiles made over dune crests and by using the hopping height model with a single velocity measurement at 3 cm above the bed. Much of the difference between the two curves can be attributed to the inclusion of form-drag from bedforms on the velocity profiles.

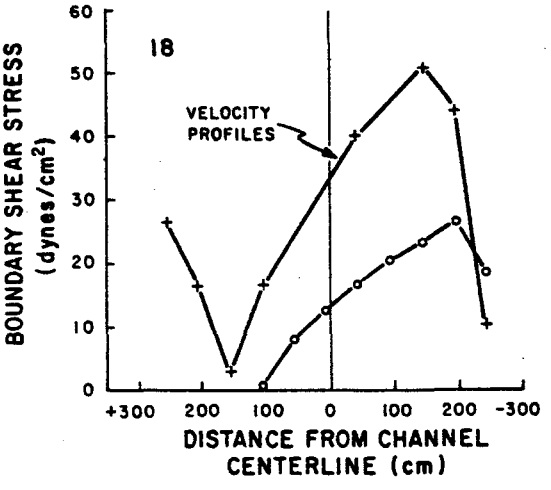

Figure 9. (continued).

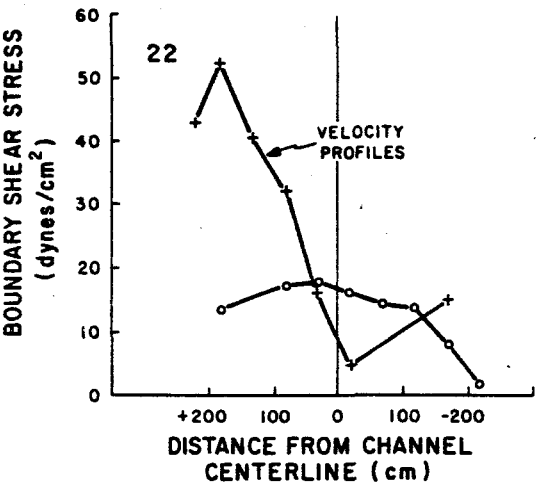

Figure 9. (continued).

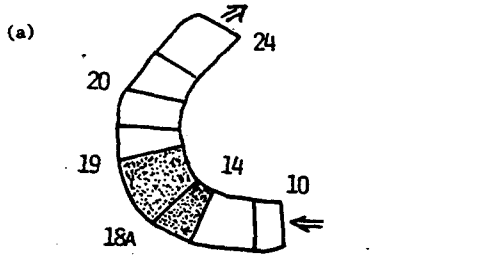

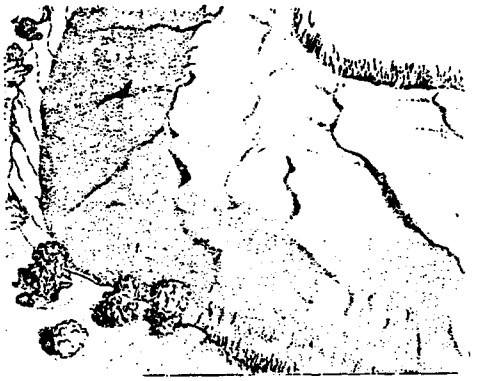

(b)

Figure 10. Sketches of stream channel and bed from left bank looking downstream at channel bed at section 14. In order to simplify portrayal of dunes along the outer bank in (b), wooden railing has been deleted from drawing. Sketches are by Lenora Wilson.

Figure 11. Sketches of stream channel and bed looking from outer bank upstream at the channel bed. Map gives location of position of viewer. (a) is the channel bed at section 19/20. In (b) left bank stake at section 20 is at the downstream end of the closest railing. Section 19/20 is near the intersection of the two railings. In (c) railing has been deleted to simplify the drawing. Sketch is from left bank at section 22.

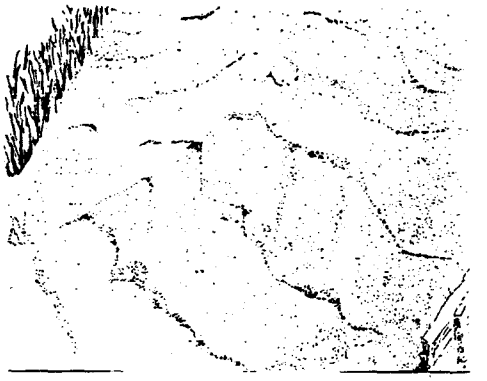

(a)

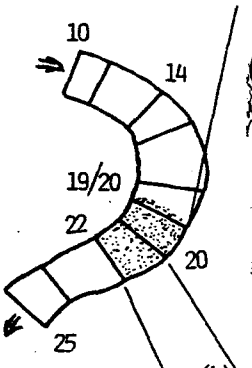

(b)

(c)

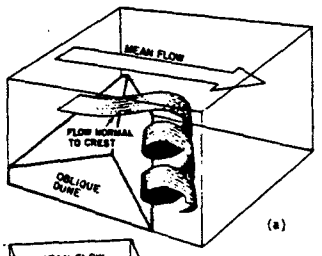

(a)

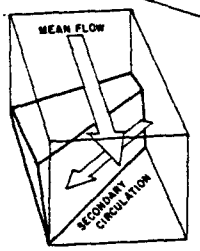

(b)

Figure 12. (a) Deflection of flow near crest, formation of separation cell and generation of cross-stream current due to bedform obliquity to mean flow.

(b) Direction of mean flow and secondary circulation induced by bedform obliquity in the trough.

(Illustrations by Leslie Reid)

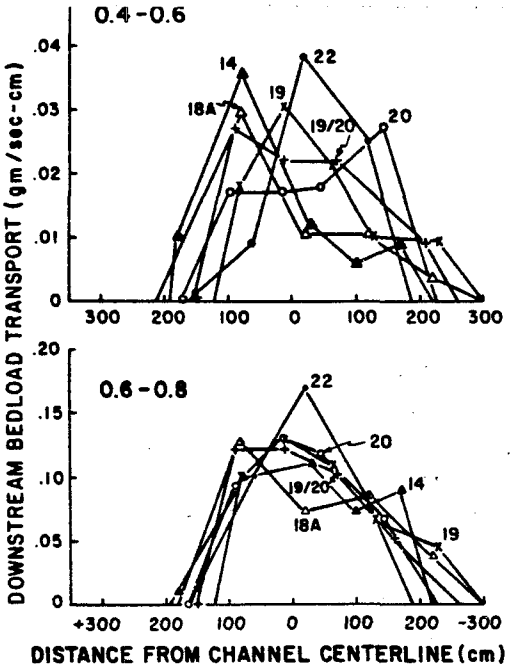

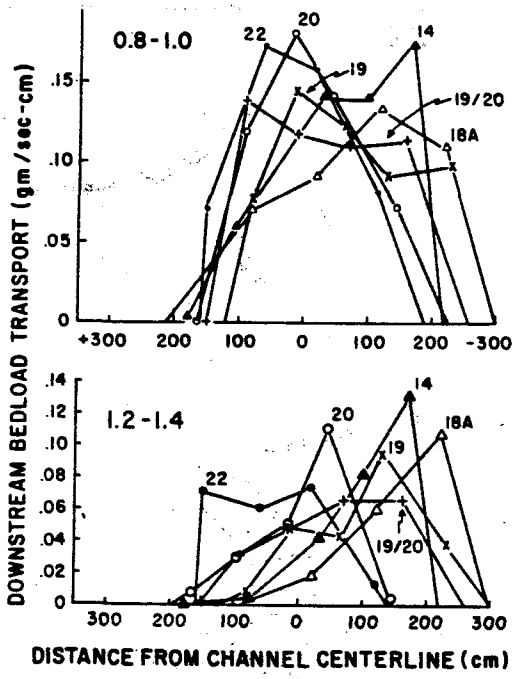

Figure 13. Downstream bedload transport fields of four $\log_{10}$ settling velocity classes through the bend. Class intervals are given in upper left corner. These four classes represent 74% of the bedload. Large numbers adjacent to curves refer to section locations shown in map. Symbols used for each curve to represent a section have the same meaning for all four graphs. Data have been normalized to have same total transport at a section as the mean for all nine sections. Variation in curves is due to structure alone; total transport is the same.

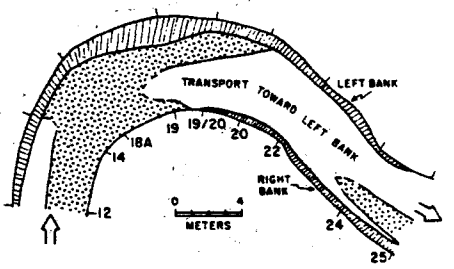

Figure 16. Direction of bedload transport in study reach. Shaded area represents bedload transport toward right bank. Clear area is bedload transport toward left bank. Dashed lines indicate uncertainty as to correct position of the boundary between fields. Diagonal lines define area occupied by submerged bank and immobile gravel.

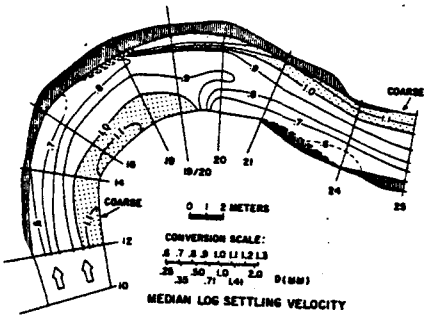

Figure 14. Map of median settling velocity distribution in bedload. Contour interval is 0.1 M_{10}. Area of dots represents immobile gravel in pool. Area with diagonal lines is submerged sloping bank with immobile sediment.

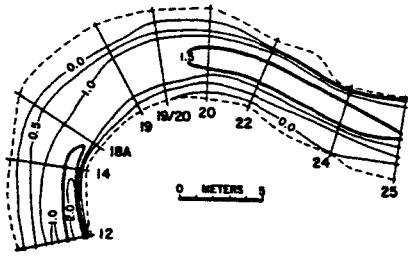

Figure 15. Bedload transport distribution in bend. Data were first corrected to give the same total discharge of 128.5 gm/sec at each section. The mean of 0.313 gm/sec-cm for the reach was then divided into each measurement to obtain the ratio used to draw the contour lines.

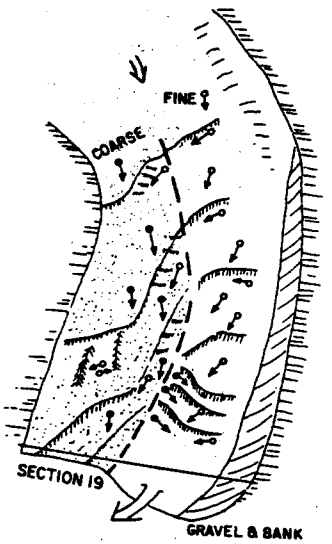

Figure 17. Summary sketch of the outward transport of coarse sediment and inward transport of fine sediment. Hachure denotes lines of dunes. Dashed line is the break in slope from the shallow point bar surface to the steep side of the bar.